Direct LDDMM of Discrete Currents with Adaptive Finite Elements

Andreas Günther, Hans Lamecker, Martin Weiser

Direct LDDMM of Discrete Currents with Adaptive Finite Elements

Andreas Günther, Hans Lamecker, and Martin Weiser

Zuse Institute Berlin, Takustraße 7, D-14195 Berlin-Dahlem, Germany
guenther@zib.de

Abstract. We consider Large Deformation Diffeomorphic Metric Mapping of general m-currents. After stating an optimization algorithm in the function space of admissable morph generating velocity fields, two innovative aspects in this framework are presented and numerically investigated: First, we spatially discretize the velocity field with conforming adaptive finite elements and discuss advantages of this new approach. Second, we directly compute the temporal evolution of discrete m-current attributes.

1 Introduction

The Large Deformation Diffeomorphic Metric Mapping (LDDMM) approach initiated in [4, 18] has attracted considerable attention over the last few years in medical imaging. It allows to match highly deformed objects and as such is capable of performing inter-individual registration. LDDMM constructs a space mapping by evolving a displacement field along a velocity field, we call *wind*. Depending on the regularity of the wind, either *diffeomorphisms* [1, 12] or *homeomorphisms* [21] of the embedded space can be obtained. Thus, it provides a basis for many applications of anatomical shape analysis, where a one-to-one correspondence between different spatial objects is required.

The LDDMM technique is commonly applied for matching *currents* [5]. Currents provide a unified mathematical description of geometrical objects of dimension 0 (points), 1 (curves), 2 (surfaces) or 3 (volumes) [7, 14] which are embedded in $\mathbb{R}^3$. The spaces of m-currents are linear and equipped with an inner product and hence are a suitable tool for statistical shape analysis [5]. The induced norm provides a similarity measure for matching of source and target objects.

In [3] a particle-mesh method has been applied to 1-currents in 2D. Therein curves of same topology represented by a parameterization were approximated by a finite point set without any tangential information regardless of some geometrical level of detail for matching. Although attaching a momentum vector at each vertex of the source shape can be proven to be the optimal wind parameterization, Cotter proposes to use cubic B-splines on a fixed grid. In an enclosed efficiency discussion this sub-optimal parameterization is still competitive due to the simpler wind structure. However the numerical scheme there relies on equidistant cartesian grids with constant diffusity in order to apply FFT techniques.

In contrast to [3] we apply in 3D the *Orthogonal Matching Pursuit* (OMP) proposed in [6] to obtain a sparse representation for general m-currents at a given geometric resolution (spectral length) in terms of a sum of discrete *Dirac delta m-currents*. Currently, the LDDMM evolution of this representation is only done indirectly via an approximative scheme [5, Rem. 4.13] as depicted in Figure 1 (left) for $m = 2$, because it would otherwise require the computation of the Jacobian of the diffeomorphism, which is a challenge when discretizing the wind using Gaussian kernels [8, 9, 19]. Furthermore, one looses the connectivity of the input mesh structure in this case. However, this is not a significant problem, since the connectivity can be recovered by applying the final displacement field to the input meshes afterwards.

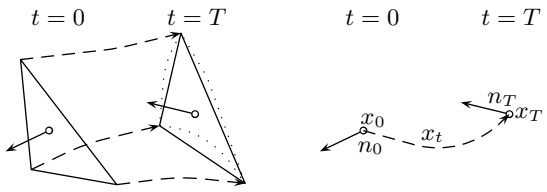

Fig. 1. Usual discrete 2-current deformation (left) versus the direct approach (right)

In this paper, we study the *direct* evolution of Dirac delta m-currents (right of Figure 1). We show that the direct approach allows to uniformly treat m-currents for $m = 0, \ldots, 3$ (Sec. 2), which to the best of our knowledge has not been shown before. We show also how to compute the Jacobian in this setting by using finite elements (FEM) to discretize the wind in the LDDMM framework (Sec. 3). Since the compactly supported basis functions are fixed in space the computation is significantly simplified. Although equidistant grids can of course be incorporated, we also in contrast to [3] consider locally refined meshes and exploit the decoupling of the wind and current discretization for an adaptive current representation, giving a significant reduction of degrees of freedom (Sec. 4). Based on our results, the increased spatial flexibility of adaptive FEM may be exploited in the future by implementing hierarchical schemes, error estimators and non-constant spatial anisotropic diffusity.

2 Continuous Matching Problem

For given shapes $\mathcal{S}, \mathcal{T} \subset \mathbb{R}^3$ we aim at constructing a sufficiently smooth bijection ϕ of $\mathbb{R}^3$ such that the distance between $\phi(\mathcal{S})$ and $\mathcal{T}$ is minimal. Here we fix the formalisms to describe the matching problem as an optimization task.

2.1 Currents

Currents are mathematical tools suited for describing geometrical objects such as points, space curves, surfaces and volumes embedded in $\mathbb{R}^3$. Their precise

definition from [7, 14] requires notation for differential forms taken from [15]. Let for $m = 0, 1, 2, 3$ the set $\mathcal{D}^m := C_c^\infty(\mathbb{R}^3, \Lambda^m\mathbb{R}^3)$ denote the vector space of all C^∞ *differential m-forms* on $\mathbb{R}^3$ with compact support. A m-current is an element of $\mathcal{D}_m$, the dual space of $\mathcal{D}^m$. The elementary *Dirac delta m-currents* $\delta_x^{u_1\wedge\ldots\wedge u_m} \in \mathcal{D}_m$ act on $\omega \in \mathcal{D}^m$ as

$$\delta_x^{u_1\wedge\ldots\wedge u_m}(\omega) = \omega(x)(u_1 \wedge \ldots \wedge u_m) \ .$$

Following the discussion in [5, Sect. 1.5.1] it turns out that for the purpose of matching currents the testspace of all C^∞ differential m-forms is not suited due to a missing bound in variation. Moreover the space $\mathcal{D}^0$ can be identified with scalar C_c^∞ functions on $\mathbb{R}^3$. For $m = 1$ and $m = 2$ the space $\mathcal{D}^m$ is isomorph to the space of vector-valued C_c^∞ functions from $\mathbb{R}^3$ to $\mathbb{R}^3$. An element of $\mathcal{D}^3$ can be written as a scalar C_c^∞ function times the determinant form on $\mathbb{R}^3$.

Both aspects motivate the use of *Reproducible Kernel Hilbert Spaces* (RKHS) W^m as testspaces.

Definition 1. *Let $d_m = 1$ for $m \in \{0, 3\}$ and $d_m = 3$ for $m \in \{1, 2\}$. For $m = 0, 1, 2, 3$ let W^m denote the dense span of d_m-vectorfields of the form $\omega(x) = k_m(x, y)a$, where $x, y \in \mathbb{R}^3$, $a \in \mathbb{R}^{d_m}$ and $k_m(x, y) = \exp(-\|x - y\|^2/\sigma_m^2)$. The space W^m can be equipped with the inner product $\langle k_m(\cdot, x)a, k_m(\cdot, y)b\rangle_{W^m} = a^* k_m(x, y)b$. Here the symbol $*$ denotes the transpose operation.*

An m-current *in $\mathbb{R}^3$ is a continuous linear functional on W^m. W_m denotes the vector space of all m-currents in $\mathbb{R}^3$.*

For $x \in \mathbb{R}^3$ and attribute *$a \in \mathbb{R}^{d_m}$ we define the elementary* Dirac delta m-currents *$\delta_x^a \in W_m$ acting on $\omega \in W^m$ as $\delta_x^a(\omega) = a^*\omega(x)$.*

The above inner product induces a norm on W^m, which can be computed efficiently via FGT even for a large number of linear combinations of the above basis functions. The chosen Gaussian kernel k_m can be considered as Green's function for some differential operator L_W (see [1, 6, 8]). With the above objects at hand the Riesz representation theorem provides a unique operator $K_W^m : W_m \to W^m$ reflecting the canonical isometry between W^m and W_m defined via

$$\langle K_W^m f, g\rangle_{W^m} = \langle f, g\rangle_{W_m, W^m} = f(g)$$

for all $f \in W_m$ and $g \in W^m$. It provides for the m-current $\mathcal{S}^m$ the Riesz representant $K_W^m\mathcal{S}^m$ as unique d_m-vectorfield on $\mathbb{R}^3$.

2.2 Homeomorphisms and Diffeomorphisms

Let Ω be an open bounded subset of $\mathbb{R}^3$ and consider functions $v_t : \bar{\Omega} \to \mathbb{R}^3$ that vanish on $\partial\Omega$. For given final time $T > 0$ and a time-dependent wind $v = (v_t)_{t\in[0,T]}$ we consider the temporal evolution of the identity map

$$\frac{\partial\phi_t^v}{\partial t} = v_t(\phi_t^v) \text{ with } \phi_0^v(x) = x \ . \tag{1}$$

In what follows it will be useful to define the *trajectory* $x_t := \phi_t^v(x)$ for some fixed space point $x \in \mathbb{R}^3$ and the map $\phi_{st}^v := \phi_t^v \circ (\phi_s^v)^{-1}$, describing the movement of a particle starting in x at time s towards $\phi_{st}^v(x)$ at time t. It is well known (see [21, Thm. C.3]), that (1) is uniquely solvable when for some $x_0 \in \Omega$ the integral $\int_0^T \|v_t(x_0)\|_{\mathbb{R}^3} + \mathrm{Lip}(v_t)\, dt$ is bounded. Furthermore its solution $\phi_t^v : \mathbb{R}^3 \to \mathbb{R}^3$ is a *homeomorphism* of Ω for all times $t \in [0,T]$. Under more restrictive assumptions onto the spatial smoothness of the wind, i.e. $v_t \in C_0^1(\Omega, \mathbb{R}^3)\ \forall t \in [0,T]$ and $\int_0^T \|v_t\|_{1,\infty}\, dt < \infty$ the unique solution of (1) is even a *diffeomorphism* of Ω for all times $t \in [0,T]$ (see [21, Thm. 8.7]). For convenience we look for the wind v_t in some Hilbert space V. Such spaces can be constructed by defining inner products associated to differential operators. Let therefore $L : V \to L^2(\mathbb{R}^3)$ be a differential operator and equip the Hilbert space V with the inner product $\langle v_t, g\rangle_V = \langle Lv_t, Lg\rangle_{L^2} = \langle L^*Lv_t, g\rangle_{V^*,V}$. Here L^* denotes the adjoint operator. For this work we use

$$S := L^*L = (-\mathrm{div}(\sigma_V^2 \nabla) + I)^k = (-\sigma_V^2 \Delta + I)^k \tag{2}$$

and $k = 1$ or $k = 2$ giving the Sobolev spaces H^k (see [8]). For given $f \in V^*$ we consider solutions $v_t \in V$ of $Sv_t = f$ with homogeneous Dirichlet boundary conditions for v_t (and v_t' if $k = 2$). Here the real parameter $\sigma_V > 0$ balances between smoothing and data fitting of the right hand side f. For other choices of L^*L and boundary conditions see [12]. Dealing with natural boundary conditions is also possible, but requires a sufficiently large domain to keep all trajectories therein. Analogous to K_W^m we introduce the isometry operator $K_V : V^* \to V$. A mathematically equivalent approach of constructing V consists in defining K_V via the Green's function $k_V(x,y)$ of L^*L, see for instance [8, 9, 19, 20].

2.3 Diffeomorphic Deformation of Currents

For $m = 0, 1, 2, 3$ let currents $\mathcal{S}^m \in W_m$ be given. Let ϕ denote a diffeomorphism on $\mathbb{R}^3$ and $d_x\phi$ the Jacobian of ϕ at x. The *pushforward* $\phi_\sharp(\mathcal{S}^m) \in W_m$ of $\mathcal{S}^m$ under ϕ is rigorously defined in [15] via the *pullback* of differential forms. For our purpose it is sufficient to mention that if $\mathcal{S}^m$ is associated to a submanifold in $\mathbb{R}^3$ its pushforward $\phi_\sharp(\mathcal{S}^m)$ under ϕ corresponds to the *deformed* submanifold $\phi(\mathcal{S}^m)$. This important property justifies to write also $\phi(\mathcal{S}^m) \in W_m$. The explicitly calculated pushforwards for elementary Dirac delta m-currents taken from [5, Table 1.2] are given in Table 1.

Table 1. Pushforwards of Dirac delta m-currents under ϕ

$m = 0$	$d_0 = 1$	$c \in \mathbb{R}$	$\phi_\sharp(\delta_x^c) = \delta_{\phi(x)}^c$
$m = 1$	$d_1 = 3$	$\tau \in \mathbb{R}^3$	$\phi_\sharp(\delta_x^\tau) = \delta_{\phi(x)}^{d_x\phi(\tau)}$
$m = 2$	$d_2 = 3$	$n \in \mathbb{R}^3$	$\phi_\sharp(\delta_x^n) = \delta_{\phi(x)}^{\lvert d_x\phi \rvert d_x\phi^{-*}(n)}$
$m = 3$	$d_3 = 1$	$\rho \in \mathbb{R}$	$\phi_\sharp(\delta_x^\rho) = \delta_{\phi(x)}^{\lvert d_x\phi \rvert \rho}$

Let some wind v be given and consider the family $(\phi_t^v)_t$ of diffeomorphisms generated via (1). The following theorem describes the direct evolution of m-current attributes $a_m \in \mathbb{R}^{d_m}$ under $(\phi_t^v)_t$, where $'$ denotes the time derivative.

Theorem 1. *The pushforwards of $\delta_{x_0}^{c_0}$, $\delta_{x_0}^{\tau_0}$, $\delta_{x_0}^{n_0}$ and $\delta_{x_0}^{\rho_0}$ under ϕ_s^v satisfying* (1) *are $\delta_{x_s}^{c_0}$, $\delta_{x_s}^{\tau_s}$, $\delta_{x_s}^{n_s}$ and $\delta_{x_s}^{\rho_s}$. Their components are given via the ODEs*

$$\begin{aligned}
x_t' &= v_t(x_t) && \text{with } x(0) = x_0\\
\tau_t' &= (d_{x_t} v_t)\tau_t && \text{with } \tau(0) = \tau_0\\
n_t' &= n_t \mathrm{tr}(d_{x_t} v_t) - (d_{x_t} v_t)^* n_t && \text{with } n(0) = n_0\\
\rho_t' &= \rho_t \mathrm{tr}(d_{x_t} v_t) && \text{with } \rho(0) = \rho_0 \ .
\end{aligned}$$

Proof. Abbreviating $J_t = d_{x_0}\phi_t^v$ and $A_t = d_{x_t} v_t$ there holds (see [1]) $J_t' = A_t J_t$ with $J(0) = I_3$. Observing the evolution of the Wronskian [13, Thm. 2.14] or via Jacobi's formula one obtains

$$|J_t|' = |J_t| \mathrm{tr}\left(J_t^{-1} J_t'\right) = |J_t| \mathrm{tr}\left(J_t^{-1} A_t J_t\right) = |J_t| \mathrm{tr}(A_t),$$

where $\mathrm{tr}(A)$ denotes the trace of a matrix A and $A^{-*} = (A^{-1})^*$. Now from Table 1 we read out

$$x_t = \phi_t^v(x_0) \ , \quad \tau_t = J_t \tau_0 \ , \quad n_t = |J_t| J_t^{-*} n_0 \ , \quad \rho_t = |J_t| \rho_0 \ .$$

Differentiation of the above equations with respect to t yields

$$\begin{aligned}
x_t' &= \phi_t^v(x_0)' = v_t(\phi_t^v(x_0)) = v_t(x_t)\\
\tau_t' &= J_t' \tau_0 = A_t J_t \tau_0 = A_t \tau_t\\
n_t' &= |J_t|' J_t^{-*} n_0 + |J_t| (J_t^{-*})' n_0 = |J_t| \mathrm{tr}(A_t) J_t^{-*} n_0 - |J_t| A_t^* J_t^{-*} n_0\\
&= n_t \mathrm{tr}(A_t) - A_t^* n_t\\
\rho_t' &= |J_t|' \rho_0 = |J_t| \mathrm{tr}(A_t) \rho_0 = \rho_t \mathrm{tr}(A_t),
\end{aligned}$$

which proves the assertion. □

Remark 1. The authors emphasize the striking advantage that Theorem 1 enables to find the final position and attribute of a Dirac delta m-current without computing the Jacobian of the deformation. The appearing ODEs only involve the Jacobian of the velocity fields, which will be given in a closed form in any case.

2.4 Optimization Problem in Function Space

Let source $\mathcal{S}^m \in W_m$ and target current $\mathcal{T}^m \in W_m$ be given for $m = 0, \dots, 3$. For given wind v we define the deformed current $\mathcal{S}_t^m := \phi_t^v(\mathcal{S}^m)$ at time t. *Matching* means the minimization of the distance of the deformed source current at final time $\mathcal{S}_T^m$ with its target current $\mathcal{T}^m$, i.e. minimizing the dual norm $\|\phi_T^v(\mathcal{S}^m) - \mathcal{T}^m\|_{W_m} = \|\mathcal{S}_T^m - \mathcal{T}^m\|_{W_m}$ in the space of m-currents.

Given a regularization parameter $\gamma > 0$ and matching weights $\omega_m \geq 0$ we consider for $v \in L^2([0,T],V)$ the following optimization problem:

$$J(v) := \gamma \int_0^T \|v_t\|_V^2 \, dt + \sum_{m=0}^{3} \omega_m \|\phi_T^v(\mathcal{S}^m) - \mathcal{T}^m\|_{W_m}^2 \to \min \quad . \tag{3}$$

Here the first summand involves the kinetic energy of the wind. The existence of a solution for (3) is proven in [10], however it is generally not unique [2]. Following [9] the gradient of J in $L^2([0,T],V)$ at fixed v is given by $(\nabla J)_t = 2\gamma v_t + 2K_V(f_t)$, where $f_t \in V^*$ is defined by

$$f_t(u) = \sum_{m=0}^{3} \omega_m \langle \mathcal{S}_t^m, \nabla (K_W^m (\mathcal{S}_T^m - \mathcal{T}^m) \circ \phi_{tT}^v)^* u \rangle_{W_m, W^m} \quad \forall u \in V \quad .$$

For further discussion concerning the choice of the gradients metric we refer the reader to [1]. With the above quantities at hand one is able to state a steepest descent optimization algorithm in the function space of velocity fields v.

3 Discrete Matching Problem

3.1 Discretization of the Wind by Finite Elements (FE)

In the field of optimal current matching mainly wind discretizations of the form

$$v_t(x) = \sum\nolimits_j k_V(x_{j,t}, x)\alpha_{j,t} \tag{4}$$

have been considered. Here $\alpha_{j,t} \in \mathbb{R}^3$ are the time-dependent momentum vectors and k_V denotes a Gaussian kernel with some global kernel parameter $\sigma_V > 0$, describing the coherent movement of neighboring particles. In order to apply *Fast Gauss Transform* (FGT) for efficient evaluation, σ_V is necessarily a constant. Although (4) can be proven to be the optimal wind parameterization, the spatial movement of non-compactly supported basis functions along trajectories $x_{j,t}$ may cause numerical difficulties. Too small distances between them cause a redundant or badly conditioned description of the velocity field while the absence of trajectories in a part of the domain produces almost no wind there for small kernel sizes. The trajectory density varies during optimization and hence is difficult to control. Because the trajectories' starting points are the spatial components of the Dirac delta source currents the number of trajectories is fixed and hence a notion of adaptivity for the velocity field can hardly be introduced. Finally, as mentioned in Sect. 2.2, C^∞ smoothness is not required to solve the evolution equation.

In [16] and [17], some of the above mentioned drawbacks are overcome by incorporating multiple kernel shapes at different scales σ_V.

Similar to the particle-mesh method proposed in [3], we follow another suboptimal approach completely decoupling the discretization of the space of m-currents W_m from the spatial velocity space V. Keeping in mind that fast point

evaluation of the wind is essential for performance, we consider adaptive hexahedral grids for Ω with hanging nodes saved as an octree. Over such hexahedral grids we construct either C^1 conforming Hermite finite elements of third order or simpler C^0 conforming Lagrange finite elements of first order. The wind for fixed time $t \in [0,T]$ in the FE basis $\{\varphi_j\}_j$ takes the form

$$v_t(x) = \sum\nolimits_{j=1}^{n} \varphi_j(x)\alpha_{j,t} \ . \tag{5}$$

In contrast to radial basis functions, locally constant functions are contained in the ansatz space and allow to represent local or even global translations with few *degrees of freedom* (DOF). Due to the compactly supported basis functions there is no need for an approximate evaluation like FGT with further unknown tolerance parameters. Since the basis functions are fixed in space, the underlying mesh provides a natural clustering which can be exploited via a smart parallel octree search algorithm for point evaluation. Furthermore this approach provides a multilevel wind hierarchy with a fraction of DOFs on the coarsest mesh level completely decoupled from the m-current discretization. These advantages also appear in the particle-mesh method with tensor-products of cubic B-splines for instance. But since we do not apply FFT for wind evaluation, we are more flexible with adaptive meshes and do not require a box domain. Moreover non-constant anisotropic diffusity $\sigma_V(x) \in \mathbb{R}^{3\times 3}$ may be incorporated in future.

A difficulty arises in the computation of the $L^2([0,T],V)$-gradient. It permanently involves the solution of a second ($k=1$) or fourth ($k=2$) order elliptic PDE in every time-step and every iteration. It is clear that one should employ suited preconditioners and / or multigrid solvers. Using existing FE libraries limits its implementation overhead. We chose libMesh [11], which provides conforming C^1 finite elements on adaptive hexahedral meshes.

The development of adaptive mesh refinement is beyond the scope of this work. Here, we provide a proof of concept that adaptive grids can easily be incorporated. Therefore we simply geometrically refine near $\mathcal{S}^m \cup \mathcal{T}^m$ considered as subsets of $\mathbb{R}^3$ equally for all times. More sophisticated error indicators suggesting refinements could be the scalar fields $|K_W^m(\mathcal{S}_T^m - \mathcal{T}^m) \circ \phi_{tT}^v|$, $|v_t|$ or $|L^*Lv_t|$. The latter one measures the smoothness of v_t. Moreover thinking of hierarchical error estimators one could compute $\|v_t^1 - I_h v_t^1\|_{L^2(Q)}$ or even $\|v_t^1 - v_t^0\|_{L^2(Q)}$ on hexahedrons Q, where v^i denote the numerical solutions for the C^i conforming FE discretization and I_h is the usual Lagrange interpolation operator.

All appearing ODEs are numerically integrated via the explicit method of Heun on an equidistant decomposition of the time interval $[0,T]$.

3.2 Current Compression and Direct Evolution

For approximating a m-current $\mathcal{S}^m \in W_m$ as $\hat{\mathcal{S}}^m = \sum_{i=1}^{s_m} \delta_{x_i}^{a_i} \in W_m$ we use the *Orthogonal Matching Pursuit* (OMP) proposed in [6]. This method iteratively selects the most important points x_i and computes corresponding attributes a_i (i.e. c_i, τ_i, n_i, ρ_i) of a general m-current via a greedy algorithm. It has the advantage of compressing the current information for a characteristical spectral

length $\sigma_m > 0$ towards a fraction. This enables the design of highly efficient numerical solution algorithms. The approximation error in OMP is controlled by a threshold parameter and the grid size of a uniform testgrid.

The obvious drawback of loosing the connectivity between vertices (for $m \geq 1$) can be compensated by applying the obtained optimal diffeomorphism to all connected vertices whenever it is required. This only requires one additional forward flow computation at the end.

In [19, Sec. 3.2] two methods to deform a 2-current $\hat{\mathcal{S}}^2$ under a family of diffeomorphisms $(\phi_t^v)_t$ are described. In contrast to all previous work, we will pursue the *direct* approach motivated by Theorem 1. For 2-currents, only 1 instead of 3 trajectories is needed to evolve the normal n_0 (Fig. 1). In general, the direct approach requires only one trajectory per attribute, hence decreasing the number of variables in the computation, whereas in the indirect case an artificial m-simplex with $m+1$ vertices is attached.

Remark 2. To quote Rem. 4.13 in [5] the direct evolution of current attributes is closer to the analytical concept of currents and is particularly suited for OMP, where no connectivity between the points is provided. But [5] indicates the need of Jacobi matrices (as they arise in Theorem 1) as a disadvantage for numerical implementation. At least for the gradient computation in the next section we benefit from the simpler structure of v_t in (5), which in Lemma 2 enables easy evaluations of $d_{x_t} v_t = \sum_{j=1}^n \alpha_{j,t} \nabla \varphi_j(x_t)^*$ and hence $\operatorname{tr}(d_{x_t} v_t)$, $(d_{x_t} v_t)w$ and $(d_{x_t} v_t)^* w$ for a vector $w \in \mathbb{R}^3$. Note that all sums over j are *local* sums due to the compact support of the basis functions φ_j.

3.3 Discrete Optimization Problem and its Gradient

Let $a(\cdot,\cdot)$ denote the bilinear form corresponding to the elliptic differential operator S from (2). We define the sparse symmetric, positive definite matrix $\mathbf{S} := [a(\varphi_i, \varphi_j)]_{i;j=1}^n$ using the FE basis $\{\varphi_j\}_j$ from Sect. 3.1. Moreover we introduce the block vectors $\boldsymbol{\alpha}_t := [\alpha_{i,t}]_{i=1}^n$, $\mathbf{x}_t := \mathbf{x}_t^m := [x_{i,t}]_{i=1}^{s_m}$ and $\mathbf{a}_t := \mathbf{a}_t^m := [a_{i,t}]_{i=1}^{s_m}$. This notation allows to write the matching terms as

$$E^m = E^m(\mathbf{x}_T, \mathbf{a}_T) = \|\phi_T^v(\hat{\mathcal{S}}^m) - \hat{\mathcal{T}}^m\|_{W_m}^2 = \|\textstyle\sum_{i=1}^{s_m} \delta_{x_{i,T}^{a_{i,T}}} - \sum_{j=1}^{r_m} \delta_{y_j}^{b_j}\|_{W_m}^2 \ .$$

Finally the discrete form of the current matching problem (3) is

$$\hat{J}(\boldsymbol{\alpha}_t) := \gamma \int_0^T \|v_t(\boldsymbol{\alpha}_t)\|_V^2 \, dt + \sum_{m=0}^3 \omega_m \|\phi_T^v(\hat{\mathcal{S}}^m) - \hat{\mathcal{T}}^m\|_{W_m}^2 \to \min$$

or even shorter via (5) and $\|v_t(\boldsymbol{\alpha}_t)\|_V^2 = a(v_t(\boldsymbol{\alpha}_t), v_t(\boldsymbol{\alpha}_t)) = \boldsymbol{\alpha}_t^* \mathbf{S} \boldsymbol{\alpha}_t$

$$\hat{J}(\boldsymbol{\alpha}_t) = \gamma \int_0^T \boldsymbol{\alpha}_t^* \mathbf{S} \boldsymbol{\alpha}_t \, dt + \sum_{m=0}^3 \omega_m E^m(\mathbf{x}_T, \mathbf{a}_T) \to \min \ . \tag{6}$$

The analytical computation of the gradient at given $\boldsymbol{\alpha}_t$ becomes manageable though the simpler wind representation (5). Numerically the computation is

more involved due to presence of Hessians of basis functions. But these are easily provided via the already mentioned libMesh library.

Theorem 2. *The gradient of $\hat{J}$ in the L^2-metric is*

$$(\nabla \hat{J})_t = 2\gamma \mathbf{S}\boldsymbol{\alpha}_t + \sum_{m=0}^{3} \omega_m((\boldsymbol{\varphi}_t^m)^* \boldsymbol{\eta}_t^m + (\partial_{\boldsymbol{\alpha}} \mathbf{g}_t^m)^* \boldsymbol{\zeta}_t^m), \tag{7}$$

$$\begin{aligned} \textit{with} \qquad \boldsymbol{\varphi}_t^m &= [\varphi_j(x_{i,t}) I_{d_m}]_{i=1\dots s_m; j=1\dots n} \\ \boldsymbol{\zeta}_t^m &= \nabla_{\mathbf{a}_T} E^m + \int_t^T (\partial_{\mathbf{a}} \mathbf{g}_s^m)^* \boldsymbol{\zeta}_s^m \, ds \\ \boldsymbol{\eta}_t^m &= \nabla_{\mathbf{x}_T} E^m + \int_t^T (\partial_{\mathbf{x}} \mathbf{g}_s^m)^* \boldsymbol{\zeta}_s^m \, ds \ . \end{aligned}$$

The proof is postponed to the appendix. The remaining quantities $\nabla_{\mathbf{x}_T} E^m, \nabla_{\mathbf{a}_T} E^m, \partial_{\boldsymbol{\alpha}} \mathbf{g}_t^m, \partial_{\mathbf{x}} \mathbf{g}_t^m$ and $\partial_{\mathbf{a}} \mathbf{g}_t^m$ from Theorem 2 for each m are specified in the next two lemmas.

Lemma 1. *Let $f_m(x) = \sum_{i=1}^{s_m} k_m(x_{i,T}, x) a_{i,T} - \sum_{j=1}^{r_m} k_m(y_j, x) b_j$. There hold*

$$\nabla_{\mathbf{x}_T} E^m = [2(d_{x_{i,T}} f_m(x_{i,T}))^* a_{i,T}]_{i=1}^{s_m} \quad \textit{and} \quad \nabla_{\mathbf{a}_T} E^m = [2 f_m(x_{i,T})]_{i=1}^{s_m} \ .$$

Proof.

$$\begin{aligned} (\partial_{x_T} E^m)\eta &= 2\left[\left(\partial_{x_T} \textstyle\sum_{i=1}^{s_m} \delta_{x_{i,T}}^{a_{i,T}}\right)\eta\right](f_m) = 2a_T^* \left(d_{x_T} f_m(x_T)\right) \eta \\ \nabla_{x_T} E^m &= 2(d_{x_T} f_m(x_T))^* a_T \\ &= 2\Big(\textstyle\sum_{i=1}^{s_m} (\nabla_2 k_m(x_{i,T}, x_T)) a_{i,T}^* - \sum_{j=1}^{r_m} (\nabla_2 k_m(y_j, x_T)) b_j^* \Big) a_T \\ (\partial_{a_T} E^m)\eta &= 2\left[\left(\partial_{a_T} \textstyle\sum_{i=1}^{s_m} \delta_{x_{i,T}}^{a_{i,T}}\right)\eta\right](f_m) = 2\eta^* f_m(x_T) \ . \end{aligned}$$

□

Lemma 2. *For $\mathbf{g}_t^m$ in (11) their sparse Jacobians are given via*

$$\begin{aligned} \mathbf{g}_t^0 &= \mathbf{0} \\ \partial_{\boldsymbol{\alpha}} \mathbf{g}_t^1 &= \left[(\tau_{i,t}^* \nabla \varphi_j(x_{i,t})) I_3\right]_{i=1\dots s_1; j=1\dots n} \\ \partial_{\boldsymbol{\alpha}} \mathbf{g}_t^2 &= \left[n_{i,t} \nabla \varphi_j(x_{i,t})^* - \nabla \varphi_j(x_{i,t}) n_{i,t}^*\right]_{i=1\dots s_2; j=1\dots n} \\ \partial_{\boldsymbol{\alpha}} \mathbf{g}_t^3 &= [\rho_{i,t} \nabla \varphi_j(x_{i,t})^*]_{i=1\dots s_3; j=1\dots n} \\ \partial_{\mathbf{x}} \mathbf{g}_t^1 &= \operatorname{diag}\Big[\textstyle\sum_{j=1}^{n} \alpha_{j,t} \tau_{i,t}^* H_{\varphi_j}(x_{i,t}) \Big]_{i=1}^{s_1} \\ \partial_{\mathbf{x}} \mathbf{g}_t^2 &= \operatorname{diag}\Big[\textstyle\sum_{j=1}^{n} n_{i,t} (\alpha_{j,t}^* H_{\varphi_j}(x_{i,t})) - (\alpha_{j,t}^* n_{i,t}) H_{\varphi_j}(x_{i,t}) \Big]_{i=1}^{s_2} \\ \partial_{\mathbf{x}} \mathbf{g}_t^3 &= \operatorname{diag}\Big[\textstyle\sum_{j=1}^{n} \rho_{i,t} \alpha_{j,t}^* H_{\varphi_j}(x_{i,t}) \Big]_{i=1}^{s_3} \\ \partial_{\boldsymbol{\tau}} \mathbf{g}_t^1 &= \operatorname{diag}\Big[\textstyle\sum_{j=1}^{n} \alpha_{j,t} \nabla \varphi_j(x_{i,t})^* \Big]_{i=1}^{s_1} \end{aligned}$$

$$\partial_{\mathbf{n}} \mathbf{g}_t^2 = \operatorname{diag}\Big[\textstyle\sum_{j=1}^n (\alpha_{j,t}^* \nabla\varphi_j(x_{i,t})) I_3 - \nabla\varphi_j(x_{i,t}) \alpha_{j,t}^* \Big]_{i=1}^{s_2}$$
$$\partial_{\boldsymbol{\rho}} \mathbf{g}_t^3 = \operatorname{diag}\Big[\textstyle\sum_{j=1}^n \alpha_{j,t}^* \nabla\varphi_j(x_{i,t}) \Big]_{i=1}^{s_3},$$

where $H_{\varphi_j}(x_{i,t})$ *denote the Hessian of* φ_j *at* $x_{i,t}$.

Proof. The proof for all cases of m can easily be adapted from the case $m = 2$. For this choice the derivatives of $\mathbf{g}_t^2$ follow from direct calculations starting with

$$\begin{aligned}
\mathbf{g}_t^2 &= \mathbf{g}^2(\boldsymbol{\alpha}_t, \mathbf{x}_t, \mathbf{n}_t) = \operatorname{diag}\left[\operatorname{tr}(d_{x_{i,t}} v_t) I_3 - (d_{x_{i,t}} v_t)^*\right]_{i=1}^{s_2} \mathbf{n}_t \\
&= \operatorname{diag}\Big[\textstyle\sum_{j=1}^n (\alpha_{j,t}^* \nabla\varphi_j(x_{i,t})) I_3 - \nabla\varphi_j(x_{i,t}) \alpha_{j,t}^* \Big]_{i=1}^{s_2} \mathbf{n}_t \\
&= \Big[\textstyle\sum_{j=1}^n n_{i,t} (\alpha_{j,t}^* \nabla\varphi_j(x_{i,t})) - \nabla\varphi_j(x_{i,t}) (\alpha_{j,t}^* n_{i,t}) \Big]_{i=1}^{s_2},
\end{aligned}$$

where $\operatorname{diag}[\mathbf{v}] = [\delta_{ij} v_i]_{i,j=1}^s$ for $\mathbf{v} \in \mathbb{R}^s$ and δ_{ij} denotes the Kronecker delta. □

Corollary 1. *If* $\omega_m = 0$ *for* $m > 0$ *Theorem 2 simply provides*

$$(\nabla \hat{J})_t = 2\gamma \mathbf{S} \boldsymbol{\alpha}_t + \omega_0 (\boldsymbol{\varphi}_t^0)^* \nabla_{\mathbf{x}_T} E^0 \quad .$$

Remark 3. The $L^2([0,T], V)$-gradient of $\hat{J}$ is immediately obtained by applying $\mathbf{S}^{-1}$ from the left in equation (7).

4 Numerical Experiments

Since the numerical implementation is not yet fully tested, we postpone the investigation of the cases $m > 0$ and only consider the case $m = 0$, i.e. $\omega_i = \delta_{i0}$. The surfaces $\mathcal{S}$ and $\mathcal{T}$ are depicted in Fig. 2. To both of them we apply the OMP with $\sigma_0 = 8$ towards $\hat{\mathcal{S}}$ with $s_0 = 1746$ points and $\hat{\mathcal{T}}$ with $r_0 = 2141$ points, which are sketched as set of spheres of diameter 8 in Fig. 3.

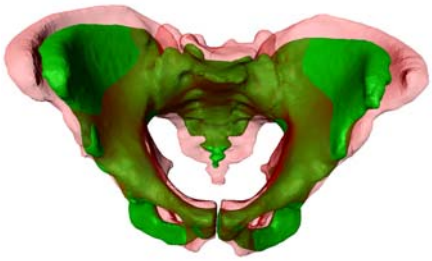

Fig. 2. $\mathcal{S}$ (dark green), $\mathcal{T}$ (light red)

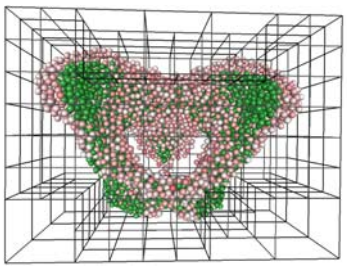

Fig. 3. $\hat{\mathcal{S}}$ (green), $\hat{\mathcal{T}}$ (red), grid

We solve the discrete matching problem (6) on $\Omega = (0, 346.56) \times (0, 205.76) \times (0, 256.96)$ with $\gamma = 0$ and tuned σ_V. For Lagrange FE ($k = 1$) on a hexahedral

adaptive grid from Fig. 3 having 568 nodes (133 of them are hanging nodes) we choose $\sigma_V = 100$. The result $\mathcal{S}_T$ is shown in Fig. 4. Secondly we solve problem (6) with Hermite FE ($k = 2$) on a uniform coarse grid having 120 nodes, whose solution is shown in Fig. 5 for $\sigma_V = 15$. Finally in Fig. 6 we compare our results with the software ExoShape[1], generating C^∞ wind via ansatz (4) with $\sigma_V = 30$. The greyscale highlights the term $\mathrm{dist}_{x\in\mathcal{S}_T}(x, \mathcal{T})$. One should keep in mind, that with $\gamma = 0$ the deformation norm vanishes in the example, but different differential operators are still present for velocity field evaluation. Although a proper comparison between all methods should use the same deformation norm $\|\cdot\|_V$, Exoshape does not easily support its change.

Fig. 4. $\mathcal{S}_T$ for C^0 wind

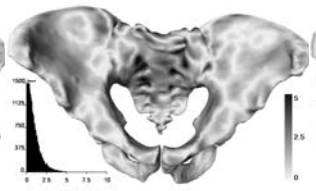

Fig. 5. $\mathcal{S}_T$ for C^1 wind

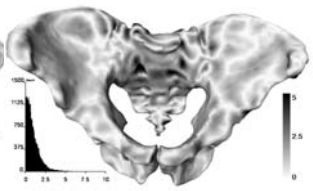

Fig. 6. $\mathcal{S}_T$ for C^∞ wind

A quantitative comparison between all different wind discretizations is issue of Table 2. Therein the column DOFs denote the number of freely choosable vectors $\alpha_{j,t}$ for fixed t. All methods provide acceptable matches with respect to the fixed level of detail $\sigma_0 = 8$. Especially the surface $\mathcal{S}_T$ corresponding to C^1 wind is also visually closest to $\mathcal{T}$ although it is obtained via less wind DOFs compared to the approach from Exoshape. This fact stresses the potential of sub-optimal, albeit simpler wind parameterizations and decoupling the discretization of the spaces W_m from V.

Table 2. One-sided surface distances between $\mathcal{S}_T$ and $\mathcal{T}$ for $m = 0$

v_t	DOFs	mean	stddev	rms	max
C^0	1·(568-133) = 435	1.18	1.14	1.64	11.33
C^1	8·120 = 960	0.95	0.91	1.32	9.16
C^∞	1746	0.97	0.93	1.34	9.70
no wind, $\mathrm{dist}_{x\in\mathcal{S}}(x, \mathcal{T})$		5.08	3.87	6.39	21.05

Appendix

In the following we prove Theorem 2.

[1] http://www-sop.inria.fr/asclepios/projects/Health-e-Child/ShapeAnalysis/

Proof. First we consider the variation of the kinetic energy, i.e. $\omega_m = 0$ for all m. One directly calculates

$$(\nabla \hat{J})_t = 2\gamma \mathbf{S}\boldsymbol{\alpha}_t \ . \tag{8}$$

Let us now consider the contrary case, i.e. $\gamma = 0$. We aim to compute $\nabla_{\boldsymbol{\alpha}} E^m$ for some fixed m. Variation of $E = E^m$ w.r.t. $\boldsymbol{\alpha}_t$ in direction $\tilde{\boldsymbol{\alpha}}_t$ gives

$$\tilde{E}^m = (\partial_{\mathbf{x}_T} E)\tilde{\mathbf{x}}_T + (\partial_{\mathbf{a}_T} E)\tilde{\mathbf{a}}_T \ . \tag{9}$$

There holds

$$\tilde{\mathbf{x}}_t = \int_0^t \tilde{v}_s(\mathbf{x}_s)\, ds = \int_0^t \boldsymbol{\varphi}_s \tilde{\boldsymbol{\alpha}}_s \, ds \ . \tag{10}$$

From Theorem 1 the evolution of m-current attributes can be written as

$$\mathbf{a}_t' = \mathbf{g}(\boldsymbol{\alpha}_t, \mathbf{x}_t, \mathbf{a}_t) = \mathbf{g}_t \quad \text{with} \quad \mathbf{a}(0) = \mathbf{a}_0 \ . \tag{11}$$

Its variation in direction $\tilde{\boldsymbol{\alpha}}_t$ satisfies

$$\tilde{\mathbf{a}}_t' = (\partial_{\boldsymbol{\alpha}} \mathbf{g}_t)\tilde{\boldsymbol{\alpha}}_t + (\partial_{\mathbf{x}} \mathbf{g}_t)\tilde{\mathbf{x}}_t + (\partial_{\mathbf{a}} \mathbf{g}_t)\tilde{\mathbf{a}}_t \quad \text{with} \quad \tilde{\mathbf{a}}(0) = 0 \ .$$

It remains to express $\tilde{\mathbf{a}}_t$. We therefore introduce the flow $\frac{dF_{st}}{dt} = (\partial_{\mathbf{a}} \mathbf{g}_t) F_{st}$ with $F_{tt} = I$ and get

$$\begin{aligned}
\tilde{\mathbf{a}}_t &= \int_0^t F_{ut}((\partial_{\boldsymbol{\alpha}} \mathbf{g}_u)\tilde{\boldsymbol{\alpha}}_u + (\partial_{\mathbf{x}} \mathbf{g}_u)\tilde{\mathbf{x}}_u)\, du \\
&= \int_0^t F_{ut}(\partial_{\boldsymbol{\alpha}} \mathbf{g}_u)\tilde{\boldsymbol{\alpha}}_u \, du + \int_0^t \int_0^u F_{ut}(\partial_{\mathbf{x}} \mathbf{g}_u)\boldsymbol{\varphi}_s \tilde{\boldsymbol{\alpha}}_s \, ds \, du \\
&= \int_0^t \left(F_{ut}(\partial_{\boldsymbol{\alpha}} \mathbf{g}_u) + \int_u^t F_{st}(\partial_{\mathbf{x}} \mathbf{g}_s)\, ds\, \boldsymbol{\varphi}_u \right) \tilde{\boldsymbol{\alpha}}_u \, du \ .
\end{aligned}$$

In particular there holds

$$\tilde{\mathbf{a}}_T = \int_0^T \left(F_{tT}(\partial_{\boldsymbol{\alpha}} \mathbf{g}_t) + \int_t^T F_{sT}(\partial_{\mathbf{x}} \mathbf{g}_s)\, ds\, \boldsymbol{\varphi}_t \right) \tilde{\boldsymbol{\alpha}}_t \, dt \ . \tag{12}$$

Combining (9), (10) and (12) we have

$$\begin{aligned}
\tilde{E}^m &= \int_0^T (\partial_{\mathbf{x}_T} E)\boldsymbol{\varphi}_t \tilde{\boldsymbol{\alpha}}_t + (\partial_{\mathbf{a}_T} E) \left(F_{tT}(\partial_{\boldsymbol{\alpha}} \mathbf{g}_t) + \int_t^T F_{sT}(\partial_{\mathbf{x}} \mathbf{g}_s)\, ds\, \boldsymbol{\varphi}_t \right) \tilde{\boldsymbol{\alpha}}_t \, dt \\
&= \int_0^T \Bigg(\underbrace{\left[(\partial_{\mathbf{x}_T} E) + \int_t^T (\partial_{\mathbf{a}_T} E) F_{sT}(\partial_{\mathbf{x}} \mathbf{g}_s)\, ds \right]}_{=:\boldsymbol{\eta}_t^*} \boldsymbol{\varphi}_t + \underbrace{(\partial_{\mathbf{a}_T} E) F_{tT}}_{=:\boldsymbol{\zeta}_t^*} (\partial_{\boldsymbol{\alpha}} \mathbf{g}_t) \Bigg) \tilde{\boldsymbol{\alpha}}_t \, dt \\
&= \int_0^T \left(\boldsymbol{\eta}_t^* \boldsymbol{\varphi}_t + \boldsymbol{\zeta}_t^* (\partial_{\boldsymbol{\alpha}} \mathbf{g}_t) \right) \tilde{\boldsymbol{\alpha}}_t \, dt \ .
\end{aligned} \tag{13}$$

Since $F_{st}F_{ts} = I$ and $\frac{dF^*_{st}}{ds} = -(\partial_{\mathbf{a}}\mathbf{g}_s)^* F^*_{st}$ we have in particular the integral form $F^*_{ts} = I + \int_t^s (\partial_{\mathbf{a}}\mathbf{g}_u)^* F^*_{us}\, du$. This helps to simplify

$$\begin{aligned}\boldsymbol{\zeta}_t &= F^*_{tT}(\nabla_{\mathbf{a}_T} E) = \Big(I + \int_t^T (\partial_{\mathbf{a}}\mathbf{g}_s)^* F^*_{sT}\, ds\Big)(\nabla_{\mathbf{a}_T} E) \\ &= \nabla_{\mathbf{a}_T} E + \int_t^T (\partial_{\mathbf{a}}\mathbf{g}_s)^* F^*_{sT}(\nabla_{\mathbf{a}_T} E)\, ds = \nabla_{\mathbf{a}_T} E + \int_t^T (\partial_{\mathbf{a}}\mathbf{g}_s)^* \boldsymbol{\zeta}_s\, ds \qquad (14)\\ \boldsymbol{\eta}_t &= \nabla_{\mathbf{x}_T} E + \int_t^T (\partial_{\mathbf{x}}\mathbf{g}_s)^* F^*_{sT}(\nabla_{\mathbf{a}_T} E)\, ds = \nabla_{\mathbf{x}_T} E + \int_t^T (\partial_{\mathbf{x}}\mathbf{g}_s)^* \boldsymbol{\zeta}_s\, ds\ . \qquad (15)\end{aligned}$$

Collecting (8), (13), (14) and (15) yields the assertion. □

Acknowledgement. We thank Stanley Durrleman from the University of Utah for the fruitful discussion and helpful suggestions at the initial phase of this paper. We further acknowledge support by DFG-MATHEON Project F2. Moreover we thank the referees for their comments which helped to improve the quality of this paper.

References

1. Beg, M.F., Miller, M.I., Trouvé, A., Younes, L.: Computing large deformation metric mappings via geodesic flows of diffeomorphisms. IJCV 61(2), 139–157 (2005)
2. Cao, Y., Miller, M.I., Winslow, R.L., Younes, L.: Large deformation diffeomorphic metric mapping of vector fields. IEEE Trans. Med. Imag. 24(9), 1216–1230 (2005)
3. Cotter, C.: The variational particle-mesh method for matching curves. Journal of Physics A: Mathematical and Theoretical 41(34), 344003 (2008)
4. Dupuis, P., Grenander, U., Miller, M.I.: Variational problems on flows of diffeomorphisms for image matching. Q. Appl. Math. 56(3), 587–600 (1998)
5. Durrleman, S.: Statistical models of currents for measuring the variability of anatomical curves, surfaces and their evolution. Phd, Univ. Nice (2010)
6. Durrleman, S., Pennec, X., Trouvé, A., Ayache, N.: Statistical models of sets of curves and surfaces based on currents. MedIA 13(5), 793–808 (2009)
7. Federer, H.: Geometric measure theory. Repr. of the 1969 ed. Classics in Mathematics. Berlin: Springer-Verlag (1996)
8. Glaunès, J., Qiu, A., Miller, M.I., Younes, L.: Large deformation diffeomorphic metric curve mapping. IJCV 80(3), 317–336 (2008)
9. Glaunès, J., Trouvé, A., Younes, L.: Diffeomorphic matching of distributions: a new approach for unlabelled point-sets and sub-manifolds matching. In: CVPR. Los Alamitos: IEEE Comput. Soc. vol. 2, pp. 712–718 (2004)
10. Glaunès, J.: Transport par difféomorphismes de points, de mesures et de courants pour la comparaison de formes et l'anatomie numérique. Ph.D. thesis, Université Paris 13 (2005)
11. Kirk, B.S., Peterson, J.W., Stogner, R.H., Carey, G.F.: `libMesh`: A C++ Library for Parallel Adaptive Mesh Refinement/Coarsening Simulations. Engineering with Computers 22(3–4), 237–254 (2006)
12. Marsland, S., Twining, C.: Constructing diffeomorphic representations for the groupwise analysis of non-rigid registrations of medical images. IEEE Trans. Med. Imag. 23(8), 1006–1020 (2004)

13. Mattheij, R.M., Molenaar, J.: Ordinary differential equations in theory and practice. Reprint of the 1996 original. Classics in Applied Mathematics. SIAM (2002)
14. Morgan, F.: Geometric measure theory. A beginner's guide. 4th ed. Elsevier (2009)
15. Morita, S.: Geometry of differential forms. American Mathematical Society (2001)
16. Risser, L., Vialard, F.X., Wolz, R., Holm, D.D., Rueckert, D.: Simultaneous fine and coarse diffeomorphic registration: Application to atrophy measurement in alzheimer's disease. In: MICCAI'10. vol. 13, pp. 610–617 (2010)
17. Sommer, S.H., Nielsen, M., Lauze, F.B., Pennec, X.: A multi-scale kernel bundle for LDDMM: Towards sparse deformation description across space and scales. In: IPMI. LNCS, Springer (2011)
18. Trouvé, A.: An infinite dimensional group approach for physics based models in pattern recognition. Tech. rep., Johns Hopkins University (1995)
19. Vaillant, M., Glaunès, J.: Surface matching via currents. In: Christensen, G.E., Sonka, M. (eds.) IPMI, LNCS, vol. 3565, pp. 381–392. Springer (2005)
20. Vaillant, M., Miller, M.I., Younes, L., Trouvé, A.: Statistics on diffeomorphisms via tangent space representations. NeuroImage 23(Supplement 1), 161–169 (2004)
21. Younes, L.: Shapes and diffeomorphisms. App. Math. Sc. 171. Springer (2010)